PCCP

Cite this: *Phys. Chem. Chem. Phys.*, 2011, **13**, 19788–19795

www.rsc.org/pccp

**PAPER**

# Proton ordering in cubic ice and hexagonal ice; a potential new ice phase—XIc†

**Zamaan Raza,[ae] Dario Alfè,[bef] Christoph G. Salzmann,[c] Jiří Klimeš,[ade] Angelos Michaelides[ade] and Ben Slater*[ae]**

***Received 4th August 2011, Accepted 21st September 2011***
**DOI: 10.1039/c1cp22506e**



Ordinary water ice forms under ambient conditions and has two polytypes, hexagonal ice (Ih) and cubic ice (Ic). From a careful comparison of proton ordering arrangements in Ih and Ic using periodic density functional theory (DFT) and diffusion Monte Carlo (DMC) approaches, we find that the most stable arrangement of water molecules in cubic ice is isoenergetic with that of the proton ordered form of hexagonal ice (known as ice XI). We denote this potential new polytype of ice XI as XIc and discuss a possible route for preparing ice XIc.

## 1 Introduction

Hexagonal ice is the most prevalent phase of ice on Earth, accounting for ~10% of its surface area and it has an important role in climatic regulation *via* albedo. Although hexagonal ice is one of the most studied materials in science, new and unusual properties are still being discovered which have implications for ice and other materials. For example, it has been recently shown that ice nucleates differently at positively and negatively charged surfaces of pyroelectric materials[1] and that the surface of crystalline ice displays a continuum of vacancy energies.[2]

Cubic ice has not been studied to the same extent, and its existence in nature is a subject of debate since it is known that Ic is metastable with respect to Ih.[3] Scheiner's halo[4] is interpreted as evidence of cubic ice in the upper atmosphere but sightings of this phenomenon are exceptionally rare,[5,6] which might suggest that Ic is not important in nature. However, a series of works have emerged, particularly in the last few years, which strongly indicate that Ic forms readily and persists under conditions characteristic of the Earth's upper atmosphere. Experiments have shown that water droplets homogeneously freeze to cubic ice at ambient pressure and temperatures between 160 K[7] and 243 K[8] and in droplets with radii in the range 5 nm[9,10] to 5 μm.[8] Whilst it was previously believed that Ic transforms rapidly to Ih at temperatures above ~180–200 K, recent studies indicate that Ic remains stable for hours at 228 K.[8] It has also been argued that differences in the surface chemistry of cubic and hexagonal ice could influence processes such as cloud formation and dehydration,[11] and ozone depletion.[12] Motivated by these recent developments, we have undertaken a basic characterisation of cubic ice using theoretical approaches.

## 2 Background

The structures of ice Ih and Ic differ only in terms of the stacking order of the puckered hexagonal bilayers that form the lattice. Both phases contain tetrahedrally coordinated water molecules forming six-membered rings, in boat and chair forms in the case of Ih and only the chair form in Ic (Fig. 1). Water molecules in both lattices must be oriented such that the "ice rules"[13] are satisfied: each oxygen atom must have two nearest neighbour hydrogens (forming a water molecule), and each oxygen–oxygen bond must be occupied by exactly one hydrogen atom, which gives rise to an intramolecular bond and an intermolecular hydrogen bond.

Although pure hexagonal ice can be isolated (within instrumental resolution), 100% cubic ice still eludes experimental synthesis. Murray and Bertram[8] have succeeded in preparing around 80% cubic ice, but the coherence of the cubic sequences was not reported and it is assumed that the cubic ice is faulted, containing irregular stacking sequences of Ih and Ic. Indeed, Kuhs *et al.*[14] assert that the stacking faults are an inherent property of ice Ic; it could be claimed that cubic ice is not a unique phase, but merely hexagonal ice containing cubic stacking faults. On the other hand, it has been proposed that the broad phase transition is a result of the defect energy at interphase grain boundaries when hexagonal ice crystals grow in bulk cubic ice.[3]

Whilst the literature contains many references to Ic, the structural integrity of the ice sample is often unknown and the Ic phase is often assumed because of the experimental regime

[a] *Department of Chemistry, University College London, 20 Gordon Street, London, WC1H 0AJ, UK. E-mail: zamaan.raza.09@ucl.ac.uk, b.slater@ucl.ac.uk*
[b] *Department of Earth Sciences, University College London, Gower Street, London, WC1E 6BT, UK*
[c] *Department of Chemistry, Durham University, South Road, Durham, DH1 3LE, UK*
[d] *London Centre for Nanotechnology, 17-19 Gordon Street, London, WC1H 0AH, UK*
[e] *Thomas Young Centre, University College London, London, WC1E 6BT, United Kingdom*
[f] *Department of Physics and Astronomy, University College London, London, WC1E 6BT, United Kingdom*
† Electronic supplementary information (ESI) available. See DOI: 10.1039/c1cp22506e

 

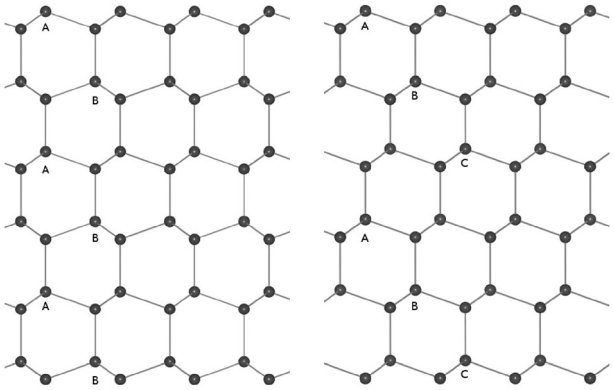


**(a)** Hexagonal ice **(b)** Cubic ice

**Fig. 1** Stacking of bilayers in hexagonal and cubic ice. The vertical is normal to the (0001) basal surface of hexagonal ice, and the (111) surface of cubic ice. Only oxygen atoms are shown, connected by hydrogen bonds.

in which the sample is prepared (*e.g.* vapour deposition at 150 K). More specifically, Dowell and Rinfret synthesized amorphous ice by condensation of water vapour onto a surface maintained below 110 K, which transformed to cubic ice on heating above 110 K,[15] identified *via* X-ray diffraction. Bertie *et al.* heated samples of high pressure ice phases II, III and V,[16] confirming the formation of cubic ice using X-ray diffraction. Steytler *et al.* cooled heavy water trapped in porous silica (containing pores with a mean diameter of 9 nm) to 260 K and identified cubic ice using neutron diffraction. Mayer and Hallbrucker reported the first unambiguous synthesis of cubic ice from liquid water by deposition of 3 μm water droplets on a cryoplate at 190 K[17] and X-ray diffraction. More recently, Murray and Bertram cooled an emulsion of pure water droplets suspended in an oil matrix, allowing an X-ray diffraction analysis of cubic ice formation as a function of temperature and droplet size.[8]

The structural integrity of ice Ic samples is not well characterised in general but it is known with certainty that Ic is metastable with respect to Ih, and anneals to ice Ih over an extended temperature range (160–240 K),[3] with no distinct phase transition. The heat of transition from cubic to hexagonal ice ($\Delta H_{c\rightarrow h}$) is extremely small; measurements vary in the range $-160$ to $-13$ J mol$^{-1}$;[17–24] increasing numbers of hexagonal sequences in the cubic ice seem to correlate with a less exothermic transition.[25] The lower free-energy of Ih is attributed to an extra water molecule in the second coordination sphere of Ih in comparison to Ic[26] (hexagonal stacking gives rise to 13 molecules in the second coordination sphere whilst the cubic sequence has 12 molecules because of the absence of a mirror plane).

We now consider the question of proton ordering in ice. It is known that proton ordering has a small but significant effect on the cohesive energy of hexagonal ice;[27] the small energy difference between cubic and hexagonal ice ($\sim$100 J mol$^{-1}$) is comparable to proton ordering energy differences in ice Ih (up to $\sim$1 kJ mol$^{-1}$),[27] although we note that proton ordering transitions occur at much lower temperatures (72 K[28] for the Ih $\rightarrow$ XI transition) than the Ic $\rightarrow$ Ih transition. Pauling was able to quantify the effect of orientational ordering on the entropy of ice[29] with a remarkable degree of accuracy. He asserted that the proton ordered configurations of ice would be degenerate, but it has since been shown that unique configurations are energetically preferred. Tajima *et al.* reported a phase transition in KOH-doped ice Ih at 72 K, associated with a loss of approximately 70% of its configurational entropy,[28] although the specifics of the proton ordered configuration remained unascertained since the X-ray diffraction techniques used lacked the resolution to characterise the hydrogen positions. Davidson and Morokuma proposed the proton ordered *antiferroelectric* $Pna2_1$ configuration[30] based on Bjerrum's model of strong and weak hydrogen bonds in water dimers;[31] it was subsequently proven, experimentally[32] and using quantum chemical simulations,[27] that the actual structure is the *ferroelectric* $Cmc2_1$ configuration.

Analyses of proton ordering in cubic ice are not unprecedented; Lekner determined that there are four proton ordered configurations for the cubic $Fd\bar{3}m$ cell, considering only ideal cells with straight hydrogen bonds, and only accounting for the Hartree component of the total energy;[33] he predicted an anti-ferroelectric ground state. In a neutron diffraction study of ice Ic, Kuhs *et al.* mentioned candidates for a hypothetical proton ordered phase with space groups $I4_1md$ and $P2_12_12_1$.[14] In a DFT study of proton ordering in hexagonal and cubic ice, Casassa *et al.* examined two cubic ice configurations with space groups $I4_1md$ (ferroelectric) and $P4_12_12$ (antiferroelectric)[34] although energies obtained for analogous calculations on hexagonal ice ($Pna2_1$ and $Cmc2_1$ forms) conflicted with those of Hirsch and Ojamäe,[27] a point they acknowledge in a later publication.[35] Casassa's results indicate that XI is metastable to the ferroelectric $I4_1md$ phase by between 880–3517 J mol$^{-1}$ which was described as 'contrary to intuition'. Given this unexpected result and the discrepancy in hexagonal ice energetics, we sought to investigate this problem to examine whether exchange–correlation functionals and the van der Waals interaction influence the proton ordering energies of hexagonal and cubic ice. In this respect, it is useful to note that very recently, Labat *et al.*[36] performed a detailed study of the $Pna2_1$ and $Cmc2_1$ forms of hexagonal ice to assess the performance of hybrid and meta-GGA (generalised gradient approximation) functionals, showing that whilst the structures and band gaps were sensitive to the functional used, the energy differences were only very weakly affected by $\sim$2 meV, in line with the notion that proton ordering energetics are well described by a range of functionals.[37]

We note in passing that the success of classical methods in predicting proton ordered configurations depends largely on the complexity of the model. The majority of widely used empirical potentials (namely SPC and the TIP*n*P family) have had little success in predicting the proton ordered configuration of ice XI, instead favouring the $Pna2_1$ antiferroelectric structure.[38,39] Only the Nada-van der Eerden (NvdE) six-site model[40] has been successful in this respect;[39] it was used to simulate ice growth on hexagonal and cubic ice substrates, the results suggesting that ice Ic is the dominant phase immediately after freezing, comprising in excess of 70% of the newly formed ice regardless of whether the substrate is cubic or hexagonal.[41] Molecular dynamics simulations of water under the influence of a static electric field unambiguously resulted in cubic ice,[42] whilst metadynamics simulations of homogeneous ice nucleation using TIP4P by Quigley and Rodger invariably demonstrated that ice Ic is the nucleating phase regardless of whether the shape of the simulation cell favoured hexagonal or cubic ice.[43] In future work,

we will report a consideration of the proton ordering energies according to commonly used forcefields to interpret whether there is an intrinsic bias in the forcefields to form cubic ice structures.

The growing interest and perceived importance of Ic coupled with the absence of characterisation studies in the literature has motivated the work described here. The main objective of this study is a systematic examination of proton ordering energetics in cubic ice using quantum chemical methods, with a comparison against the relatively well characterised hexagonal ice. The success of DFT in predicting the $Cmc2_1$ structure of ice XI[27] and the correct ground state of other proton ordered ice[44,45] reassures us that the proton ordering energies of cubic ice can be predicted.

## 3 Model and computational details

For hexagonal ice, 16 symmetry-unique eight-molecule proton ordered configurations as determined by Hirsch and Ojamäe[27] were considered. The ice Ic cell contains eight molecules, and is cubic with a side length of 6.358 Å and space group $Fd\bar{3}m$;[26] this cell has only 4 symmetry-unique proton ordered configurations, one of which is antiferroelectric. By cutting through the (011) plane, it is possible to construct a four molecule tetragonal cell of dimensions (4.4958 Å × 4.4958 Å × 6.3580 Å) which also has four proton ordered configurations; the advantage of this cell is that a 2 × 1 × 1 supercell has 11 proton ordered configurations, two of which are antiferroelectric, and is comparable to the eight-molecule orthorhombic hexagonal ice cell used by Hirsch and Ojamäe. Symmetry unique proton ordered configurations that satisfy the ice rules were generated using graph invariant software provided by Knight, Beck and Singer.[45–48]

DFT calculations were conducted using the plane wave VASP code and the Quickstep[49] module of the CP2K suite. CP2K uses a hybrid Gaussian/plane wave (GPW) representation which is very computationally efficient.[50] Wavefunctions were represented using the triple-ζ doubly polarised (TZV2P) basis set, and the electron density using a plane wave expansion with a 450 Ry cutoff and Goedecker–Teter–Hutter (GTH) norm-conserving pseudopotentials.[51] The Perdew–Burke–Ernzerhof (PBE) GGA exchange–correlation functional was used for calculations without a dispersion correction, since it has been shown to describe hydrogen bonding energetics in ice I well,[52,53] with a small but consistent 5% overbinding.[54] Application of a dispersion correction directly to the PBE functional would exacerbate overbinding, so for comparison, Grimme's DFT-D3 correction[55] was used in conjunction with the Becke–Lee–Yang–Parr (BLYP) GGA functional. BLYP systematically underbinds ice but it performs well for hydrogen-bonded systems when dispersion is taken into account.[56] A dispersion cutoff of 12 Å was used, but the repulsive 3-body C9 term of DFT-D3 was omitted because it only reduced the extent of the underbinding slightly, at a significant computational cost.

CP2K currently only supports Γ-point sampling, so all eight-molecule cells were replicated to construct 3 × 2 × 2 hexagonal ice (smallest lattice parameter of 13.48 Å) and 2 × 3 × 2 cubic ice (12.46 Å) supercells containing 96 molecules. In all cases, full cell relaxation and geometry optimisation were performed in the absence of any symmetry constraints.

In order to gauge the impact of basis set completeness and basis set superposition error (BSSE), the CP2K PBE calculations for all hexagonal and cubic ice cells were repeated using the plane wave code VASP. The projector-augmented wave (PAW) method was used,[57] a plane wave cutoff of 550 eV and a 6 × 3 × 3 (54 k-points) for hexagonal ice or 3 × 6 × 4 (72 k-points) for cubic ice Monkhorst-Pack grid of k-points were employed. Additional high precision calculations were performed on the ground state cubic and hexagonal configurations using hard PAW potentials, a cutoff of 1000 eV and 128 k-points (a 8 × 4 × 4 grid for hexagonal ice or 4 × 8 × 4 for cubic ice). In addition, a number of approaches were compared to examine the importance of van der Waals interactions and electron delocalisation within the two polytypes; these include GGA (the PBE functional), the van der Waals density functional[58] using an optimised PBE exchange functional (optPBE-vdW)[59] and PBE with 25% Hartree–Fock exchange (PBE0). The van der Waals density functional calculations were performed in VASP, using the self-consistent implementation of Klimeš *et al.*[60]

As an independent quantum mechanical reference, we have also performed diffusion Monte Carlo (DMC) calculations using the Casino code,[61] with Dirac–Fock pseudopotentials.[62] The core radii of the oxygen and the hydrogen pseudopotentials were 0.4 Å and 0.26 Å, respectively. The trial wavefunctions were of the Slater-Jastrow type, with a single Slater determinant. The single particle orbitals were obtained from DFT-LDA plane-wave calculations using the PWscf code,[63] with a plane-wave cutoff of 300 Ry, and were re-expanded in B-splines.[64]

Extensive time step tests have been performed on the ice VIII and the ice II structures near their equilibrium volume, using the primitive cells in both cases. The results of these tests have been reported in detail,[65] and we found that using a time step of 0.002 a.u., together with the locality approximation,[66] cohesive energy differences between ice II and VIII were converged to within ~5 meV molecule$^{-1}$ and hence this setup was used in the calculations described here. The DMC calculations were performed on supercells of dimensions 3 × 2 × 2 and 2 × 3 × 2 for the XI and XIc structures, respectively, containing 96 water molecules in both cases. We used the Model Periodic Coulomb (MPC) technique to treat the electron–electron interactions, which helps to significantly reduce DMC size errors.[67] Size tests performed on the VIII and the II structures[65] showed that, with cells including 96 molecules or more, finite size errors are reduced to less than 5 meV molecule$^{-1}$.

All relaxed structures are given in the ESI.†

## 4 Results and discussion

We begin by comparing the periodic density functional evaluation of the cohesive energy,‡ 27 distinct proton ordering arrangements for hexagonal and cubic ice were considered

‡ In the DFT calculations reported here, the internal energy is used to determine the cohesive energies. Here we define the cohesive energy as the energy liberated when gaseous water molecules condense to form the ice lattice. Assuming a pressure of 1 bar and a cell volume of 250 Å$^3$, the contribution from the $pV$ term is of the order of 2 J mol$^{-1}$. Considering the cell volume varies by no more than 0.1% between proton ordered configurations, it is clear that the contribution to the enthalpic energy difference is negligible being less than 0.01 J mol$^{-1}$.

 

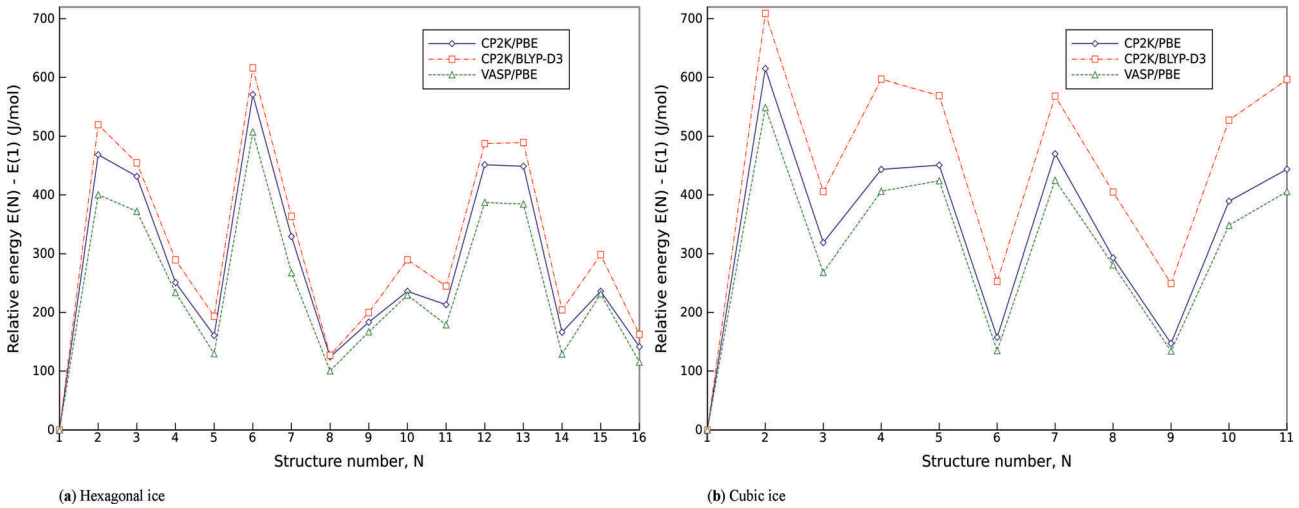


**Fig. 2** Relative energies for 16 hexagonal and 11 cubic symmetry-unique proton ordered configurations, as calculated using DFT. Energies are shown relative to structure 1 in both cases. The connecting lines have no physical meaning, and are present to guide the eye. In a, structure 1 is the experimentally verified $Cmc2_1$ structure of ice XI, and 2 is the antiferroelectric $Pna2_1$ configuration predicted by Davidson and Morokuma.[30] In b, structure 1 is the ground state $I4_1md$ structure, according to PBE and BLYP-D3 calculations, and can be considered the cubic analogue of ice XI.

using the GPW method (CP2K) and plane wave approaches using the PBE functional. In order to account for the effect of dispersion in an explicit way, the BLYP-D3 formulation was also used to evaluate the proton ordering energies. In Fig. 2, it is seen that qualitatively and quantitatively, the PBE results obtained using CP2K and VASP are very similar, underlining that the GPW method is reliable for discriminating between extremely small energy differences on the J mol$^{-1}$ scale. The figure also shows that BLYP-D3 gives a very similar relative energy distribution for the different structures considered indicating that in these very closely related structures, differences in the dispersion energy are to a first approximation negligible. Note that PBE overbinds at hydrogen bonding distances, mimicking the binding energy due to short-range dispersion. In the BLYP-D3 approach, an empirically parameterised function which has a $\frac{1}{r^6}$ dependence describing short and long range dispersions is used.

We now consider the data in Fig. 2 in combination with the cohesive energies shown in Tables 1 and 2. In the case of hexagonal ice, cohesive energies are shown relative to structure 1 (the $Cmc2_1$ configuration of ice XI, Fig. 3a) which clearly has the lowest cohesive energy of the hexagonal structures, in agreement with the calculations of Hirsch and Ojamäe[27] and Tribello and Slater.[37] The qualitative shape of the graph is similar to the one published by Hirsch and Ojamäe, and quantitative differences are attributed to differences in the basis set quality and k-point sampling used. The value for the cohesive energy of ice XI obtained here, −67.76 kJ mol$^{-1}$, compares favourably with the −68.1 kJ mol$^{-1}$ reported by Pan *et al.*,[53] also using CP2K but with a slightly lower plane wave cutoff.

No experimental estimate of the ice XI cohesive energy exists to our knowledge—proton disordered Ih is recorded to have a cohesive energy of 58.95 kJ mol$^{-1}$ [4] and Johari estimated an enthalpy change for the transition of around 250 J mol$^{-1}$,[3] suggesting the cohesive energy of ice XI should be 59.25 kJ mol$^{-1}$. In recent work,[2] we found a very similar value for proton disordered Ih to that reported here of −67.3 kJ mol$^{-1}$ and Pan *et al.*[68] reported an energy range of around 500 J mol$^{-1}$ depending upon the degree of proton disorder. Hence the absolute cohesive energies according to PBE are overestimated with respect to literature values for ice. Nevertheless, as reported in Tribello and Slater[37] and underlined by the comparison of PBE and BLYP-D3 data, the variation in proton ordering energies is not sensitive to the functional used since the predominant difference to the total energy is electrostatic. Note that our energy difference between the $Cmc2_1$ and $Pna2_1$ structures ($N$ = 1 and 2, respectively, on Table 1) using PBE give an energy difference of around 400 J mol$^{-1}$ which compares well with the recent estimate of 335 J mol$^{-1}$ reported by Labat *et al.*[36]

Given that the hexagonal ice results are consistent with our previous work and that of Hirsch and Ojamäe, the cubic ice relative energies can be viewed with confidence. According to Table 2, the lowest energy configuration of cubic ice has

**Table 1** DFT cell optimised cohesive energies for all symmetry-unique proton ordered hexagonal ice configurations

| | | DFT cohesive energy/kJ mol$^{-1}$ | | |
|---|---|---|---|---|
| N | Space group | CP2K/PBE | CP2K/BLYP-D3 | VASP/PBE |
| 1 | $Cmc2_1$ | −67.901 | −69.434 | −64.503 |
| 2 | $Pna2_1$ | −67.432 | −68.914 | −64.102 |
| 3 | $Pna2_1$ | −67.470 | −68.979 | −64.131 |
| 4 | $Pbn2_1$ | −67.650 | −69.144 | −64.268 |
| 5 | $Pca2_1$ | −67.740 | −69.241 | −64.373 |
| 6 | $P2_12_12_1$ | −67.330 | −68.818 | −63.995 |
| 7 | $P2_12_12_1$ | −67.572 | −69.070 | −64.235 |
| 8 | $Cc$ | −67.777 | −69.307 | −64.402 |
| 9 | $Pc$ | −67.718 | −69.234 | −64.336 |
| 10 | $Pc$ | −67.665 | −69.144 | −64.273 |
| 11 | $Pc$ | −67.688 | −69.189 | −64.324 |
| 12 | $P2_1$ | −67.450 | −68.946 | −64.115 |
| 13 | $P2_1$ | −67.452 | −68.945 | −64.118 |
| 14 | $P2_1$ | −67.735 | −69.230 | −64.374 |
| 15 | $P2_1$ | −67.665 | −69.136 | −64.271 |
| 16 | $P1$ | −67.760 | −69.272 | −64.387 |

**Table 2** DFT cell optimised cohesive energies for all symmetry-unique proton ordered cubic ice configurations

| | | DFT cohesive energy/kJ mol$^{-1}$ | | |
|---|---|---|---|---|
| N | Space group | CP2K/PBE | CP2K/BLYP-D3 | VASP/PBE |
| 1 | $I4_1md$ | −67.797 | −69.021 | −64.087 |
| 2 | $P4_12_12$ | −67.182 | −68.312 | −63.538 |
| 3 | $Pna2_1$ | −67.479 | −68.615 | −63.818 |
| 4 | $Pna2_1$ | −67.354 | −68.424 | −63.680 |
| 5 | $Pmn2_1$ | −67.346 | −68.452 | −63.663 |
| 6 | $Pca2_1$ | −67.640 | −68.768 | −63.952 |
| 7 | $P2_12_12$ | −67.327 | −68.453 | −63.662 |
| 8 | $Pc$ | −67.504 | −68.616 | −63.806 |
| 9 | $Pc$ | −67.650 | −68.771 | −63.953 |
| 10 | $P2_1$ | −67.408 | −68.493 | −63.738 |
| 11 | $P2_1$ | −67.353 | −68.424 | −63.681 |

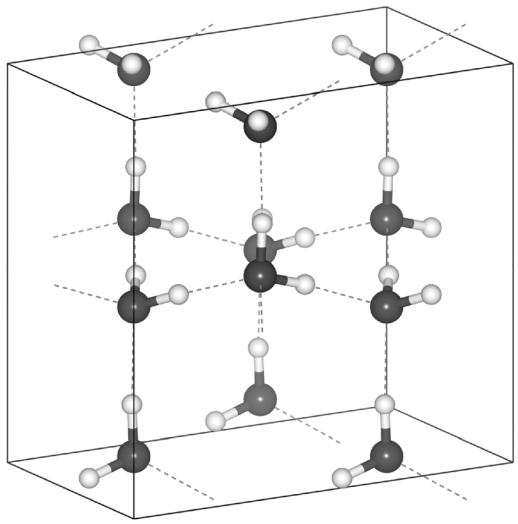

**(a)** Ice XIh ($Cmc2_1$)

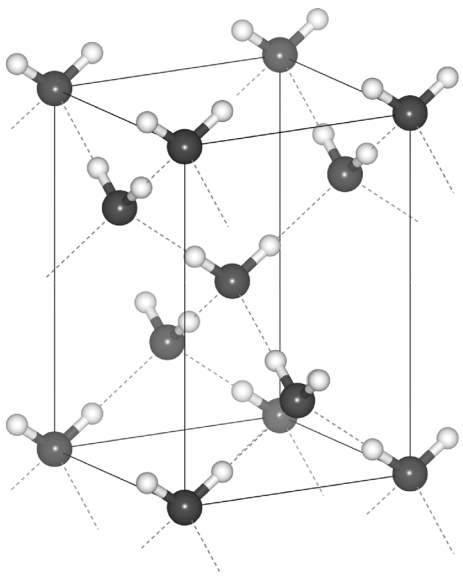

**(b)** Ice XIc ($I4_1md$)

**Fig. 3** DFT ferroelectric ground state structures of ice Ih (XIh) and ice Ic (XIc). Although the tetragonal four molecule cell of XIc is shown, a 2 × 1 × 1 supercell was generated to enumerate proton ordered configurations and calculate energies.

$I4_1md$ symmetry (Fig. 3b), is ferroelectric (only structures 2 and 7 are antiferroelectric) and consists of 100% inverse centre-symmetric ("h-cis") dimers—according to Bjerrum's classification.[31]

We henceforth refer to the ground state $I4_1md$ structure as "ice XIc", where we retain the c subscript to denote cubic stacking of the layers, despite the fact that the ground state ordered configuration has a tetragonal unit cell ($I4_1md$ is in fact a subgroup of $Fd\bar{3}m$, the space group of the cubic ice cell). In order to avoid ambiguity, we will refer to the proton ordered $Cmc2_1$ form as "ice XIh." The hydrogen bond network topology of the ice XIc structures is in fact identical to that of a sub-lattice of the well-characterised ice VIII—the proton ordered variant of ice VII, which consists of two independent interpenetrating ice Ic lattices. However, the ice VIII lattice is antiferroelectric overall because the dipole moments of the two sub-lattices exactly cancel one another. XIc exhibits maximum polarisation where all dipoles are aligned along the $c$-axis which results in an exceptionally high molecular dipole moment of 3.56 Debye, in comparison to 3.46 Debye for XIh.

The datasets for cubic and hexagonal ice are internally consistent and agree on the ground state configurations, but do not agree on the magnitude of the energy difference between ice XIh and XIc. GPW calculations indicate that ice XIh has a lower cohesive energy than XIc by 102 J mol$^{-1}$ but the plane wave approach yields a much larger difference of $\Delta H_{c\rightarrow h} \simeq -416$ J mol$^{-1}$. This order of stability disagrees with the findings of Casassa *et al.*[34] but because of the acute sensitivity of this problem, we were motivated to perform very high precision calculations using the plane wave approach to eliminate the basis set superposition errors inherent in the GPW approach. All of the remaining results refer to hard potential, PAW plane wave calculations and DMC calculations. Estimates of the cohesive energy according to DMC were obtained from an equation of state fit using the data reported in Fig. 4.

From Table 3 it is clear that accurate estimates of the energy difference between XIh and XIc are much smaller than those reported in Tables 1 and 2. The functional with the most sophisticated treatment of dispersion, optPBE-vdW has the most negative value, predicting that XIc is metastable with

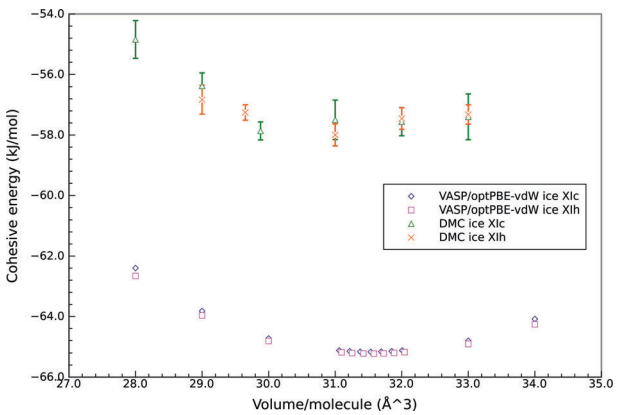


**Fig. 4** Equation of state plot for ice XIc and XIh, calculated using the optPBE-vdW functional and DMC.

**Table 3** Comparison of ice XIh and ice XIc energies and structures obtained with VASP using hard PAW potentials and DMC

| | Cohesive energy/kJ mol$^{-1}$ | | Volume/$H_2O$/Å$^3$ | | OĤO bond angle (°) | | |
|---|---|---|---|---|---|---|---|
| Density functional | Ice XIh | Ice XIc | Ice XIh | Ice XIc | Ice XIh | Ice XIc | $\Delta H_{c\rightarrow h}$/J mol$^{-1}$ |
| PBE | −61.312 | −61.359 | 30.41 | 30.35 | 177.28 | 177.66 | +47 |
| optPBE-vdW | −65.388 | −65.359 | 31.58 | 31.53 | 177.08 | 177.36 | −29 |
| PBE0 | −62.630 | −62.684 | 30.02 | 30.17 | 177.60 | 178.25 | +54 |
| DMC | −57.80 ± 0.17 | −57.84 ± 0.22 | 31.18 ± 0.22 | 31.28 ± 0.31 | — | — | +40 ± 280 |



respect to XIh. *Total* energies from BLYP-D2 (Grimme's original correction)[69] and PBE0 (with 25% Hartree–Fock exchange) calculations yield similar values (+12 J mol$^{-1}$ and +54 J mol$^{-1}$ respectively) which suggest that XIh is metastable with respect to XIc. The PBE energy difference obtained is very similar to that of PBE0, suggesting that moderate levels of non-local exchange have very little effect on the energy difference between proton ordered hexagonal and cubic ice. However, both optPBE-vdW and BLYP-D2 reduce the energy difference between XIc and XIh more directly, where, as already noted, it would appear van der Waals terms stabilise XIh with respect to XIc. Turning to DMC, XIc has the lowest cohesive energy obtained with DMC but the error bars overlap with those of XIh and the energies were obtained from single point energy evaluations of relaxed plane wave PBE geometries.

PBE and the optPBE-vdW density functional approaches suggest that XIc has a lower density than XIh with disagreement between the order of stability. As already noted, PBE over-binds at small hydrogen-bonding distances and thus mimics short-range vdW attraction but neglects long-range attraction. By comparison, optPBE-vdW explicitly models both short and long-range dispersion contributions and thus, we assume, stabilises XIh with respect to XIc because of the additional molecule in the second coordination shell, despite the fact that XIc is predicted to be the denser phase. PBE0 does not account for dispersive interactions and produces a more localised density distribution resulting in an enhanced electrostatic contribution to the cohesive energy, yielding XIh as the denser and more stable phase. This is perhaps surprising given that dipole moment in XIc is 0.1 Debye larger, which could be expected to give rise to an enhanced electrostatic energy for XIc, possibly explaining the PBE0 result since exact exchange favours a more localised and ionic electronic structure.

It is known that the zero point energy is sizable in ice and hence the zero point energy difference could influence the relative stability of XIc and XIh. From four point numerical derivative vibrational calculations using the PBE (hard pseudopotential) optimised structures, it was found that the zero point energy of XIc is 133.349 kJ mol$^{-1}$, 125 J mol$^{-1}$ greater than that for XIh. Hence $\Delta H_{c\rightarrow h}$ is modified to −78 J mol$^{-1}$, yielding XIh as the more stable phase. However, using ultrasoft pseudopotentials with the PBE functional and the CASTEP code[70] tells a different story: a zero point energy difference of 467 J mol$^{-1}$ combined with a $\Delta H_{c\rightarrow h}$ of −130 J mol$^{-1}$ strongly stabilises cubic ice. Considering that we are unable to distinguish the energies of XIh and XIc with the approaches used here, it seems premature to interpret the zero point energy differences given that these are quantities which are dependent on the second derivative of the energy.

Turning now to configurational entropy, in the tetrahedrally coordinated lattice characteristic of both phases, there are six possible orientations of each molecule, resulting in $6^8$ = 1 679 616 configurations in an eight-molecule cell. For both phases, only 114 of these are permitted by the ice rules, but most of these configurations are related by symmetry operations; in the case of XIh, six of these 114 have the ground state $Cmc2_1$ structure, whilst for XIc, six ground state structures have the $I4_1md$ space group. Thus there are six ways of generating both XIh and XIc cells and it can be concluded that they have identical configurational entropies.

For each functional the densest phase reassuringly has the smallest first nearest neighbour oxygen–oxygen separation. Turning now to hydrogen bonds, we have recently demonstrated that there is a strong correlation between the hydrogen bond angle and energy;[71] more specifically the linearity of the OĤO bond is an excellent indicator of stability. For all of the functionals used here, XIc has a mean hydrogen bond angle closest to 180° with a smaller variance in the hydrogen bonding angle than XIh, evidence that XIc should be the most stable. Only when dispersive interactions are taken into account does XIh become stable with respect to XIc. It would appear that the order of stability is very subtly influenced by the composition of the functional recipe. Within the limits of accuracy associated with our functionals, we conclude that XIc and XIh are approximately isoenergetic. This interpretation is supported by the DMC energies which are also separated by just 40 J mol$^{-1}$ albeit with a substantial error bar.

## 5 Conclusions

The ferroelectric $I4_1md$ configuration (polarised in the *c* direction) is identified as the unambiguous ground state proton ordered phase of cubic ice, XIc, having the lowest cohesive energy according to PBE and BLYP-D3 calculations. Higher precision plane wave calculations suggest that ice XIc is comparable in energy to ice XIh where the difference in energy is of the order of tens of J mol$^{-1}$. The best approximation to an accurate van der Waals functional, optPBE-vdW, confirms that energy difference between XIh and XIc is on the J mol$^{-1}$ energy scale. DMC calculations show that within the intrinsic error bars, the XIh and XIc are isoenergetic. The conclusion from all of the high precision DFT and DMC calculations is that ice XIh and XIc are essentially isoenergetic within the confidence limits and intrinsic errors associated with the approaches used here.

It seems reasonable to contend that XIc should be a competitive phase to XIh and that in principle, Ic should transform to XIc. The relative energies of the second most favourable arrangement of protons in both phases are dissimilar, amounting to ∼130 J mol$^{-1}$ for XIh and ∼270 J mol$^{-1}$ for XIc. This may indicate that the transformation to XIc may be more facile than for XIh, since the potential well separating the

ground state from the next most favourable level is deeper for XIc than for the XIh phase.

To observe XIc in a physical experiment, one would first need to prepare reasonably pure Ic, which appears to be extremely difficult within the laboratory. Ice XIII, XIV[25] and XV[72] have been successfully isolated by very slow cooling (to prevent transformation to Ih and then XIh) in the presence of dopants. If pure Ic can be prepared, we tentatively suggest that it may be transformed into XIc in this manner.

## Acknowledgements

BS and AM acknowledge the award of a DTA studentship for ZR. ZR and BS wish to thank Chris Knight and Sherwin Singer for providing graph invariant software used in this work. We acknowledge the use of UCL computer resources and the national facility HECToR *via* our membership of UK's Materials Chemistry Consortium, which is funded by EPSRC (EP/F067496). The work of DA is supported by a EURYI award as provided by EPSRC (www.esf.org/euryi). DMC calculations were performed on the Oak Ridge Leadership Computing Facility, located in the National Center for Computational Sciences at Oak Ridge National Laboratory, which is supported by the Office of Science of the Department of Energy under Contract DE-AC05-00OR22725 (USA). JK is grateful to UCL and the EPSRC for support through the PhD+ scheme. AM is supported by the EPSRC, and the European Research Council.

## References

1 D. Ehre, E. Lavert, M. Lahav and I. Lubomirsky, *Science*, 2010, **327**, 672–675.
2 M. Watkins, D. Pan, E. G. Wang, A. Michaelides, J. VandeVondele and B. Slater, *Nat. Mater.*, 2011, **10**, 794–798, submitted.
3 G. P. Johari, *Philos. Mag. B*, 1998, **78**, 375–383.
4 V. F. Petrenko and R. W. Whitworth, *Physics of Ice*, Oxford University Press, 1999.
5 E. Whalley, *Science*, 1981, **211**, 389–390.
6 E. Whalley, *J. Phys. Chem.*, 1983, **87**, 4174–4179.
7 W. Zhang, C. He, J. Lian and Q. Jiang, *Chem. Phys. Lett.*, 2006, **421**, 251–255.
8 B. J. Murray and A. K. Bertram, *Phys. Chem. Chem. Phys.*, 2006, **8**, 186–192.
9 J. Jelassi, H. L. Castricum, M. Bellissent-Funel, J. Dore, J. B. W. Webber and R. Sridi-Dorbez, *Phys. Chem. Chem. Phys.*, 2010, **12**, 2838–2849.
10 E. B. Moore, E. de la Llave, K. Welke, D. A. Scherlis and V. Molinero, *Phys. Chem. Chem. Phys.*, 2010, **12**, 4124–4134.
11 D. M. Murphy, *Geophys. Res. Lett.*, 2003, **30**, 2230.
12 B. J. Murray, D. A. Knopf and A. K. Bertram, *Nature*, 2005, **434**, 202–205.
13 J. D. Bernal and R. H. Fowler, *J. Chem. Phys.*, 1933, **1**, 515.
14 W. F. Kuhs, D. V. Bliss and J. L. Finney, *J. Phys. Colloq.*, 1987, **3**, 631.
15 L. G. Dowell and A. P. Rinfret, *Nature*, 1960, **188**, 1144–1148.
16 J. E. Bertie, L. D. Calvert and E. Whalley, *J. Chem. Phys.*, 1963, **38**, 840.
17 E. Mayer and A. Hallbrucker, *Nature*, 1987, **325**, 601–602.
18 Y. P. Handa, D. D. Klug and E. Whalley, *Can. J. Chem.*, 1988, **66**, 919–924.
19 C. G. Salzmann, E. Mayer and A. Hallbrucker, *Phys. Chem. Chem. Phys.*, 2004, **6**, 1269.
20 O. Yamamuro, *J. Phys. Chem. Solids*, 1987, **48**, 935–942.
21 Y. P. Handa, D. D. Klug and E. Whalley, *J. Chem. Phys.*, 1986, **84**, 7009.
22 J. A. McMillan and S. C. Los, *Nature*, 1965, **206**, 806–807.
23 H. Sugisaki, H. Suga and S. Seki, *Bull. Chem. Soc. Jpn.*, 1968, **41**, 2591–2599.
24 J. E. Shilling, M. A. Tolbert, O. B. Toon, E. J. Jensen, B. J. Murray and A. K. Bertram, *Geophys. Res. Lett.*, 2006, **33**, 0–4.
25 C. G. Salzmann, P. G. Radaelli, A. Hallbrucker, E. Mayer and J. L. Finney, *Science*, 2006, **311**, 1758–1761.
26 M. Chaplin, *Water Structure and Science (accessed 06/2011)*.
27 T. K. Hirsch and L. Ojamäe, *J. Phys. Chem. B*, 2004, **108**, 15856–15864.
28 Y. Tajima, T. Matsuo and H. Suga, *Nature*, 1982, **299**, 810–812.
29 L. Pauling, *J. Am.Chem. Soc.*, 1935, **57**, 2680–2684.
30 E. R. Davidson and K. Morokuma, *J. Chem. Phys.*, 1984, **81**, 3741.
31 N. Bjerrum, *Science*, 1952, **115**, 385.
32 S. M. Jackson, V. M. Nield, R. W. Whitworth, M. Oguro and C. C. Wilson, *J. Phys. Chem. B*, 1997, **101**, 6142–6145.
33 J. Lekner, *Physica B (Amsterdam)*, 1997, **240**, 263–272.
34 S. Casassa, M. Calatayud, K. Doll, C. Minot and C. Pisani, *Chem. Phys. Lett.*, 2005, **409**, 110–117.
35 A. Erba, S. Casassa, R. Dovesi, L. Maschio and C. Pisani, *J. Chem. Phys.*, 2009, **130**, 074505.
36 F. Labat, C. Pouchan, C. Adamo and G. E. Scuseria, *J. Comput. Chem.*, 2011, **32**, 2177–2185.
37 G. A. Tribello and B. Slater, *Chem. Phys. Lett.*, 2006, **425**, 246–250.
38 V. Buch, P. Sandler and J. Sadlej, *J. Phys. Chem. B*, 1998, **102**, 8641–8653.
39 S. W. Rick, *J. Chem. Phys.*, 2005, **122**, 094504.
40 H. Nada and J. P. J. M. van der Eerden, *J. Chem. Phys.*, 2003, **118**, 7401.
41 M. A. Carignano, *J. Phys. Chem. C*, 2007, **111**, 501–504.
42 I. M. Svishchev and P. G. Kusalik, *Phys. Rev. Lett.*, 1994, **73**, 975–979.
43 D. Quigley and P. M. Rodger, *J. Chem. Phys.*, 2008, **128**, 154518.
44 G. A. Tribello, B. Slater and C. G. Salzmann, *J. Am. Chem. Soc.*, 2006, **128**, 12594–12595.
45 C. Knight, S. J. Singer, J. L. Kuo, T. Hirsch, L. Ojamäe and M. Klein, *Phys. Rev. E: Stat., Nonlinear, Soft Matter Phys.*, 2006, **73**, 056113.
46 J. L. Kuo, J. V. Coe, S. J. Singer, Y. B. Band and L. Ojamäe, *J. Chem. Phys.*, 2001, **114**, 2527.
47 J. L. Kuo and S. J. Singer, *Phys. Rev. E: Stat. Phys., Plasmas, Fluids, Relat. Interdiscip. Top.*, 2003, **67**, 16114.
48 C. Knight and S. J. Singer, *J. Chem. Phys.*, 2008, **129**, 164513.
49 J. VandeVondele, M. Krack, F. Mohamed, M. Parrinello, T. Chassaing and J. Hutter, *Comput. Phys. Commun.*, 2005, **167**, 103–128.
50 G. Lippert, J. Hutter and M. Parrinello, *Mol. Phys.*, 1997, **92**, 477–487.
51 S. Goedecker, M. Teter and J. Hutter, *Phys. Rev. B: Condens. Matter*, 1996, **54**, 1703–1710.
52 D. R. Hamann, *Phys. Rev. B: Condens. Matter*, 1997, **55**, R10157–R10160.
53 D. Pan, L. M. Liu, G. A. Tribello, B. Slater, A. Michaelides and E. Wang, *J. Phys.: Condens. Matter*, 2010, **22**, 074209.
54 P. J. Feibelman, *Phys. Chem. Chem. Phys.*, 2008, **10**, 4688–4691.
55 S. Grimme, J. Antony, S. Ehrlich and H. Krieg, *J. Chem. Phys.*, 2010, **132**, 154104.
56 B. Santra, A. Michaelides, M. Fuchs, A. Tkatchenko, C. Filippi and M. Scheffler, *J. Chem. Phys.*, 2008, **129**, 194111.
57 G. Kresse and D. Joubert, *Phys. Rev. B: Condens. Matter Mater. Phys.*, 1999, **59**, 1758–1775.
58 M. Dion, H. Rydberg, E. Schröder, D. Langreth and B. Lundqvist, *Phys. Rev. Lett.*, 2004, **92**, 22–25.
59 J. Klimeš, D. R. Bowler and A. Michaelides, *J. Phys.: Condens. Matter*, 2010, **22**, 022201.
60 J. Klimeš, D. Bowler and A. Michaelides, *Phys. Rev. B: Condens. Matter Mater. Phys.*, 2011, **83**, 195131.
61 R. J. Needs, M. D. Towler, N. D. Drummond and P. López Ros, *J. Phys.: Condens. Matter*, 2010, **22**, 023201.
62 J. R. Trail and R. J. Needs, *J. Chem. Phys.*, 2005, **122**, 174109.
63 P. Giannozzi, S. Baroni, N. Bonini, M. Calandra, R. Car, C. Cavazzoni, D. Ceresoli, G. L. Chiarotti, M. Cococcioni, I. Dabo, A. Dal Corso, S. de Gironcoli, S. Fabris, G. Fratesi, R. Gebauer, U. Gerstmann, C. Gougoussis, A. Kokalj, M. Lazzeri,



 

L. Martin-Samos, N. Marzari, F. Mauri, R. Mazzarello, S. Paolini, A. Pasquarello, L. Paulatto, C. Sbraccia, S. Scandolo, G. Sclauzero, A. P. Seitsonen, A. Smogunov, P. Umari and R. M. Wentzcovitch, *J. Phys.: Condens. Matter*, 2009, **21**, 395502.
64 D. Alfè and M. Gillan, *Phys. Rev. B: Condens. Matter Mater. Phys.*, 2004, **70**, 161101.
65 B. Santra, J. Klimeš, D. Alfè, A. Tkatchenko, B. Slater, A. Michaelides, R. Car and M. Scheffler, *Phys. Rev. Lett.*, 2011, in press, to be published on the 28th October 2011.
66 L. Mitáš, E. L. Shirley and D. M. Ceperley, *J. Chem. Phys.*, 1991, **95**, 3467–3475.
67 L. M. Fraser, W. M. C. Foulkes, G. Rajagopal, R. J. Needs, S. D. Kenny and A. J. Williamson, *Phys. Rev. B: Condens. Matter*, 1996, **53**, 1814–1832.
68 D. Pan, L. M. Liu, G. A. Tribello, B. Slater, A. Michaelides and E. Wang, *Phys. Rev. Lett.*, 2008, **101**, 155703.
69 S. Grimme, *J. Comput. Chem.*, 2006, **27**, 1789–1799.
70 M. D. Segall, P. J. D. Lindan, M. J. Probert, C. J. Pickard, P. J. Hasnip, S. J. Clark and M. C. Payne, *J. Phys.: Condens. Matter*, 2002, **14**, 2717.
71 G. A. Tribello, B. Slater, M. A. Zwijnenburg and R. G. Bell, *Phys. Chem. Chem. Phys.*, 2010, **12**, 8597–8606.
72 C. G. Salzmann, P. Radaelli, E. Mayer and J. Finney, *Phys. Rev. Lett.*, 2009, **103**, 15701.